Biomedical Signal Processing and Control 38 (2017) 44–54

Contents lists available at ScienceDirect

Biomedical Signal Processing and Control

journal homepage: www.elsevier.com/locate/bspc

A discretized tomographic image reconstruction based upon total variation regularization

Ezgi Demircan-Tureyen [a,*], Mustafa E. Kamasak [b]

[a] Faculty of Engineering, Dept. of Computer Engineering, Istanbul Kultur University, Istanbul 34156, Turkey
[b] Faculty of Computer and Informatics, Dept. of Computer Engineering, Istanbul Technical University, Istanbul 34390, Turkey

ARTICLE INFO

Article history:
Received 27 July 2016
Received in revised form 11 February 2017
Accepted 29 March 2017
Available online 20 May 2017

Keywords:
Tomographic reconstruction
Discrete tomography
Total variation
Regularization
Segmentation

ABSTRACT

Tomographic image reconstruction problem has an ill-posed nature like many other linear inverse problems in the image processing domain. Discrete tomography (DT) techniques are developed to cope with this drawback by utilizing the discreteness of an image. Discrete algebraic reconstruction technique (DART) is a DT technique that alternates between an inversion stage, employed by the algebraic reconstruction methods (ARM), and a discretization (i.e. segmentation) stage. Total variation (TV) minimization is another popular technique that deals with the ill-posedness by exploiting the piece-wise constancy of the image and basically requires to solve a convex optimization problem. In this paper, we propose an algorithm which also performs the successive sequences of inversion and discretization, but it estimates the continuous reconstructions under TV-based regularization instead of using ARM. Our algorithm incorporates the DART's idea of reducing the number of unknowns through the subsequent iterations, with a 1-D TV-based setting. As a second contribution, we also suggest a procedure to be able to select the segmentation parameters automatically which can be applied when the gray levels (corresponding to the different densities in the scanned object) are not known a priori. We performed various experiments using different phantoms, to show the proposed algorithm reveals better approximations when compared to DART, as well as three other continuous reconstruction techniques. While investigating the performances, we considered limited number of projections, limited-view, noisy projections and lack of prior knowledge on gray levels scenarios.

1. Introduction

Sparsity of the observed data and the existence of the noise are the main drawbacks of a typical linear inverse problem. In the field of image processing, there exist many such problems (e.g. denoising, deblurring, inpainting, and tomographic reconstruction) having such drawbacks which cause ill-posedness. To be able to cope with that inherent nature of them, some prior knowledge is exploited. For example, if an image is known to be sparse in a certain domain, then an appropriate regularization can be used to enforce this sparsity. Likewise, if the image is known to have only a few discrete intensity levels, those levels can directly be used as a constraint to improve the inversion process. Total variation (TV) based regularization is a popular example to the former one. It exploits the sparsity in the gradient domain and enforces piecewise-constancy (PWC) while preserving the edges. On the other hand, discrete tomography (DT) is an example to the latter one. It is specifically used for tomographic image reconstruction, which refers to the reconstruction of the axial slice images of an object whose projections are collected by a projection technique such as computed tomography (CT), electron tomography (ET), and positron emission tomography (PET). DT basically utilizes the discreteness of the image, to be able to handle the incomplete projection data. Incompleteness of the projection data is a frequent phenomenon in tomography, due to many physical limitations, as well as the need for reducing the radiation dose.

The problem of reconstructing images from their projections can either be solved analytically, or algebraically. Filtered back projection (FBP) is a conventional analytical method which is based on central slice theorem [1]. FBP is still widely used due to its fast and simple computation, despite its low quality reconstructions. Algebraic reconstruction methods (ARM), on the other hand, treat the problem as a system of linear equations and solve it with iterative projections on the hyperplanes whose intersection corresponds to the solution. Algebraic reconstruction technique (ART)

* Corresponding author.
E-mail addresses: e.demircan@iku.edu.tr (E. Demircan-Tureyen), kamasak@itu.edu.tr (M.E. Kamasak).

http://dx.doi.org/10.1016/j.bspc.2017.03.015
1746-8094/

has numerous variations such as simultaneous iterative reconstruction technique (SIRT), simultaneous algebraic reconstruction technique (SART) [2] (see [3] for a comprehensive list of ART derived algorithms). However, these methods cannot produce satisfying reconstructions when the data is incomplete. TV-based methods and DT techniques aim to handle such cases to be able to reconstruct an image from its incomplete projections.

In many applications of tomography (e.g. non destructive test – NDT), the object of interest is restricted to a small number of different attenuation coefficients, therefore the *range* of the unknown image is a discrete valued set with a few number of different levels. Current DT methods basically take the advantage of this prior knowledge. However, it worths mentioning that, another variant of DT was originally defined by Herman and Kuba [4,5], as a field that deals with an image function with discrete valued *domain*, which is a finite subset of the integer *lattice*. There are many strategies used to solve both variants of DT problems, such as handling it as a combinatorial problem and modeling it using network flows [6,7] or graph-cuts for implicit labeling as in [8], approximating the solution statistically (e.g. maximum a posteriori probability (MAP) estimate) by fitting the problem to a probability distribution [9], or combining a continuous reconstruction process with a subsequent discretization step as Batenburg and Sijbers did in [10]. In [10], the discrete algebraic reconstruction technique (DART), whose labeling strategy forms the backbone of this study, was proposed. This technique alternates between a continuous algebraic reconstruction stage (SART in [10] and SIRT in a later paper [11] on DART) and a segmentation phase (a simple global thresholding scheme in [10] and projection distance minimization (PDM) as a criterion for adaptive thresholding and automatic gray level estimation in [11]), in an iterative manner. The original DART algorithm assumes that the gray levels of the unknown image are known in advance. In this study, we will also first assume that the gray levels are known, in order to show the utility of the proposed reconstruction algorithm by comparing it to the DART; but then we will propose a method to estimate the segmentation parameters to be used when we have no knowledge of what the gray levels are. Furthermore, the DART algorithm has the ability of reducing the number of unknowns by updating the pixels that are typically on the boundary region where the reconstruction tends to fail. The DART keeps updating them within the subsequent iterations, while fixing the other ones. This strategy reduces the number of variables, yet the problem becomes less under-determined and can be solved more accurately. This property is also preserved within the proposed method.

Modeling the image reconstruction problem under TV-based regularization mostly requires to solve an optimization problem with an unconstrained cost functional consisting of an L^2 data fidelity term, in order to enforce fidelity to the observed data, and an isotropic or anisotropic TV term, in order to enforce PWC. The concept of using such a model in imaging problems was first suggested by Rudin et al. [12] (later referred to as ROF model), where they introduced isotropic TV as an edge preserving measure. In ROF model, both functions, therefore their summation, are convex which makes a reliable optimization possible. However, the TV measure is non-differentiable, which makes its optimization hard. In [12], the ROF model for the denoising problem is solved by guaranteeing convergence, but suffering from high computational cost. Thereafter, various TV solvers have been developed in order to accelerate it. Chambolle proposed a faster convergent algorithm to minimize TV by considering a dual formulation, which originates the idea of projected gradients [13]. In [14], a numerical scheme (see [15]) was used to fasten Chambolle's method, and its application to the deconvolution problem was realized. In [16], Goldstein and Osher introduced split Bregman technique to be used an anisotropic TV-based denoising problem. Also, the alternating direction method of multipliers (ADMM), which introduced in 1970s but re-invented multiple times in different fields, is frequently employed in the literature, as a variant of augmented Lagrangian (see [17] for well-known numerical schemes using augmented Lagrangian). In [18], an ADMM algorithm was proposed for various TV-based convex optimization problems. In [19], an application of ADMM to TV-based tomographic reconstruction is realized. We also preferred to use a publicly available TV solver (named TVAL3) [20], which performs an ADMM algorithm. Furthermore, while we are working on this paper, a paper which also improves the capabilities of DART by using TV is published (see [21]). It disparately models the discrete tomography problem as a TV-regularized non-convex optimization problem, consisting of a soft segmentation function which allows automated labeling, and solves the problem by using non-convex optimization techniques.

In this paper, we propose an algorithm which incorporates a TV-based reconstruction stage and a segmentation procedure, successively. While applying these decomposed sequences of inversion and discretization, we also reduce the number of unknowns in the linear system by exploiting the idea originally proposed by DART. We also suggest a segmentation procedure. The overall algorithm will be called as discretized – total variation based iterative reconstruction technique (D-TVIRT). The paper is organized as follows: Section 2 introduces the problem of interest, and reviews the DART algorithm and TV minimization technique, respectively. Section 3 presents the proposed algorithm by subdividing into modules. In Section 4, the experiments and their results are provided. Section 5 discusses the findings and finally, Section 6 concludes the paper.

2. Methods

2.1. Problem definition and notation

The problem of tomographic reconstruction is considered as a system of linear equations, where the equations are corresponding to the projection measurements and the unknown variables are the discrete pixel intensity levels. The measurements are corresponding to the detector values collected from different angles by rotating an X-ray source around the object of interest. Let $\boldsymbol{x} \in \mathbb{R}^N_{\geq 0}$ be a 1-D representation of a 2-D image $\boldsymbol{X} \in \mathbb{R}^{\sqrt{N}\times\sqrt{N}}_{\geq 0}$, and $\boldsymbol{b} \in \mathbb{R}^M_{\geq 0}$ be the projection measurements (i.e. sinogram). We denote the linear sensing operator by $\boldsymbol{A} \in \mathbb{R}^{M\times N}_{\geq 0} : \mathbb{R}^N \to \mathbb{R}^M$, which maps an image to the projection domain, and the noise vector by $\boldsymbol{\eta}$.

$$\boldsymbol{b} = \boldsymbol{A}\boldsymbol{x} + \boldsymbol{\eta} \tag{1}$$

This is a linear inverse problem where $\boldsymbol{x}$ is tried to be estimated from the observation $\boldsymbol{b}$, by using a known system matrix $\boldsymbol{A}$ and some prior information on $\boldsymbol{x}$. Here, two difficulties can be indicated: One, due to the existence of the noise $\boldsymbol{\eta}$, $\boldsymbol{b}$ cannot be a continuous function of $\boldsymbol{x}$, even $\boldsymbol{A}$ is invertible. Second, having fewer projection data than the discretization points yields the system under-determined. As it was introduced in the previous section, DT methods cope with the latter difficulty by exploiting the discreteness of the intensities. By the assumption of having a few discrete intensity values that are known in advance, the quality of the reconstruction can strongly be improved. For this discrete-valued problem, let $\boldsymbol{x}_j \in \{\xi_1, \xi_2, \ldots, \xi_L\}$, where $\xi_{l\in\{1,2,\ldots,L\}}$ is one of the gray levels, which we will call as *label* while mentioning discretization.

2.2. DART algorithm

The DART algorithm employs algebraic reconstruction methods and global thresholding based segmentation, successively. Former step computes the inversion without an explicit regularization, while the later step discretizes the estimate to a pre-determined

set of labels. In [10], the SART algorithm [2] was used as the continuous, algebraic reconstruction subroutine and a simple global thresholding scheme, which uses the average of consecutive gray levels, for segmentation.

Here, a brief explanation on the DART algorithm is given step by step. DART starts with an initial estimate by performing the SART and carries out the following steps iteratively:

(1) Reconstructed image $\boldsymbol{x}^{(k)}$ is segmented, so that the resulting image $\boldsymbol{s}^{(k)}$ has only the gray levels $s_j^{(k)} \in \mathcal{L}$, where the label set $\mathcal{L} = \{\xi_1, \xi_2, \ldots, \xi_L\}$.
(2) From $\boldsymbol{s}^{(k)}$, *boundary pixels* in $\boldsymbol{B}^{(k)}$, which differ from at least one of its adjacent pixels (in the 8-connected neighborhood), are determined. Then, these pixels are extended with a randomized scheme which includes a non-boundary pixel to the set of $\boldsymbol{B}^{(k)}$ with $1-p$ probability, where $p \in [0,1]$ is called as *fix probability*. This new set $\boldsymbol{U}^{(k)}$ includes *update pixels*, that are the only pixels which will be updated in the next iteration, while the remaining *fixed pixels* in $\boldsymbol{F}^{(k)} = \{1, 2, \ldots, N\} \setminus \boldsymbol{U}^{(k)}$ are not changed.
(3) Residual sinogram $\boldsymbol{r}^{(k)}$ is computed, by subtracting the forward projection of the image of fixed pixels $\boldsymbol{f}^{(k)}$ from the projection data as:

$$\boldsymbol{r}^{(k)} = \boldsymbol{b} - \boldsymbol{A}\boldsymbol{f}^{(k)}, \boldsymbol{f}_j^{(k)} = \begin{cases} \boldsymbol{s}_j^{(k)}, & j \in \boldsymbol{F}^{(k)} \\ 0, & \text{otherwise} \end{cases} \tag{2}$$

(4) The SART algorithm is then applied on $\boldsymbol{r}^{(k)}$ to update $\boldsymbol{u}^{(k)}$, which denotes the sub-image consisting of the update pixels in $\boldsymbol{U}^{(k)}$, and added on the image with fixed intensities as follows:

$$\boldsymbol{x}^{(k+1)} = \boldsymbol{f}^{(k)} + SART(\boldsymbol{u}^{(k)}, \boldsymbol{A_j} \in \boldsymbol{U}^{(k)}, \boldsymbol{r}^{(k)})\boldsymbol{u}_j^{(k)} = \begin{cases} \boldsymbol{x}_j^{(k)}, & j \in \boldsymbol{U}^{(k)} \\ 0, & \text{otherwise} \end{cases} \tag{3}$$

In this equation, $SART(\boldsymbol{u}^{(k)}, \boldsymbol{A_j} \in \boldsymbol{U}^{(k)}, \boldsymbol{r}^{(k)})$ denotes image reconstruction obtained by SART algorithm using $\boldsymbol{u}^{(k)}$ as the initial image, $\boldsymbol{A_j} \in \boldsymbol{U}^{(k)}$ as the system matrix for the update pixels, and $\boldsymbol{r}^{(k)}$ as the projections.
(5) Finally, Gaussian smoothing filter with standard deviation of σ pixels (denoted as G_σ) is applied and return back to step (1) as long as the termination criterion is not met.

DART reduces the number of unknowns in the original underdetermined system, since the succeeding iterations come up with a problem to be solved for only a few pixels (the pixels in $\boldsymbol{U}^{(k)}$). This strategy not only improves the computational cost, but also yields more accurate results since the system becomes less underdetermined if the fixed pixels are set to the correct levels.

2.3. TV Minimization

The theory of compressed sensing (CS) [22] states that the reconstruction of a signal from insufficient data (according to Nyquist–Shannon criteria) is possible under some assumptions, such as sparsity. Hence, the signal recovery methods based on CS seek for the most sparse solution. These methods typically use L^1 as a surrogate for L^0 [22], [23], or use L^2-norms (known as Tikhonov regularization) to be minimized. TV-norm is another popular measure that is used to regularize many ill-posed inverse problems, especially on the images. Basic foundation of TV regularization is the assumption of having sparse images in the gradient domain. Using TV measure as regularizer, instead of the other L^1- or L^2-minimization methods, makes the reconstructed images sharper since the high frequency regions are highly preserved [12]. Let the operator $\Delta : \mathbb{R}^{\sqrt{N}\times\sqrt{N}} \to \mathbb{R}^{\sqrt{N}\times\sqrt{N}} \times \mathbb{R}^{\sqrt{N}\times\sqrt{N}}$ be a difference operator which operates on a 2D image $\boldsymbol{X}$ in matrix form. Then, the anisotropic TV (that we will be using) is defined as follows:

$$\|\boldsymbol{x}\|_{TV} := \sum_{i,j} |\Delta \boldsymbol{X}_{i,j}| = \sum_{i,j} (|\Delta_1 \boldsymbol{X}_{i,j}| + |\Delta_2 \boldsymbol{X}_{i,j}|) \tag{4}$$

where Δ_1 and Δ_2 are two components of Δ, denoting the horizontal and vertical differences, respectively, and defined as follows:

$$\Delta_1 \boldsymbol{X}_{i,j} = \boldsymbol{X}_{i,j} - \boldsymbol{X}_{i-1,j}, \ \Delta_2 \boldsymbol{X}_{i,j} = \boldsymbol{X}_{i,j} - \boldsymbol{X}_{i,j-1} \tag{5}$$

The estimation of the underlying x in Eq. (1) under TV-based regularization requires to minimize the following functional:

$$J(\boldsymbol{x}) = \frac{1}{2}\|\boldsymbol{A}\boldsymbol{x} - \boldsymbol{y}\|_2^2 + \lambda \|\boldsymbol{x}\|_{TV} \tag{6}$$

Here, the first, quadratic term of the objective function is known as data fidelity term which ensures the fidelity to the observation. The second term is the TV-norm as the prior on the original image, multiplied by a regularization parameter $\lambda > 0$ that balances the importance of the two terms. The optimization problem that should be solved is given below:

$$\boldsymbol{x}^* = \underset{\boldsymbol{x} \in \mathbb{R}^N}{arg\,\min} \ J(\boldsymbol{x}) \tag{7}$$

where $\boldsymbol{x}^*$ is the estimate.

The problem given in Eq. (7) is computationally hard to solve due to the non-differentiability and non-smoothness of the TV term. Fortunately, TV and therefore $J(x)$ are convex, so Eq. (7) can be interpreted in terms of convex optimization and solved by using convex optimization tools. Many of such tools produce significantly fast results by utilizing the idea of splitting. They split the problem into either differentiable or non-differentiable sub-problems, and solves those new simpler problems. In this paper, we used TVAL3 [20] solver which provides an efficient algorithm by splitting and alternating between the sub-problems to minimize a TV-based augmented Lagrangian functional.

3. Proposed method

In this section, we propose an algorithm which incorporates DART with TV-based regularization, by employing TV-regularized minimization instead of the algebraic reconstruction stages of the DART. The motivation is taking the advantages of both techniques: the DART's ability of producing more accurate and robust results when compared to the continuous reconstruction techniques finalized by a segmentation stage, and the TV minimization's ability of preventing local minima and producing sharper, therefore easier to segment results with effectively suppressed noise. The success of DART is based on the idea of alternating between the inversion and the discretization stages, the latter of which guides the inversion by enforcing a-priori gray levels, and the idea of unknown reduction by only focusing to the boundaries, which yields a less under-determined system of linear equations. On the other hand, the success of TV minimization is based on imposing PWC when the signal is known to be sparse in the gradient domain. This study makes use of these two techniques by embedding 2-D and 1-D TV regularizations to the appropriate stages of the DART algorithm. The algorithm is first presented module by module, and then summarized in the third subsection. As declared before, we call our algorithm as discretized-TV based iterative reconstruction technique (D-TVIRT).

3.1. TV-based reconstruction

The DART algorithm starts with a fixed number of SART iterations to compute an initial estimate. In order to ensure a better initial guess, we suggested to replace the SART stage with a TV

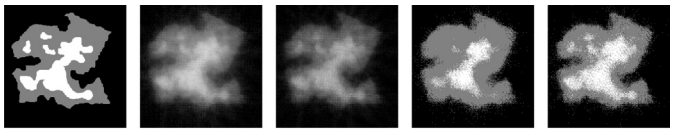

Fig. 1. Comparison of using SART and TV minimization for initial estimate. (a) original phantom (b) ten iterations of SART reconstruction, (c) maximum five iterations of TV minimization reconstruction, (d) segmented (b), and (e) segmented (c) using simple global thresholding scheme used in DART.

minimization stage in [24]. In Fig. 1, SART and TV minimization reconstruction methods are separately applied on the observed 15-projection sinogram of the multi-label phantom adapted from [10] and given in Fig. 1(a). In this paper, we suggest using TV minimization technique for every subsequent continuous reconstruction phases of DART, instead of SART or any other algebraic reconstruction methods. In other words, we suggest combining the pattern of discretization followed by the DART algorithm, with a TV-based regularization scheme.

The subsequent iterations of DART reduces the set of unknown pixels to a subset of the update pixels (recall that the update pixels were the boundary pixels plus some randomly selected pixels). Since TV is a variational measure which is defined as the integral of the gradient of the image, it is not applicable for a disjointed subset of the pixels. This is the case for 2-D TV. However, by treating that subset as a 1-D signal, one can apply 1-D TV regularization on it. Here the problem is how to organize the update pixels so that the resulting 1-D signal can be regarded as piece-wise constant. For that purpose, our algorithm first performs binary connected component labeling on the update pixels u and assigns each pixel to its associated component $\boldsymbol{c_k}$. In other words, all connected pixels are grouped into c_ks, where $k \in \{1, 2, \ldots, \kappa\}$ for κ independent connected components, and ordered separately. Once they are formed, 1-D TV regularization is performed on a concatenated vector of those $\boldsymbol{c_k}$s. The model is defined as follows:

$$\boldsymbol{u^*} = arg\min_{\boldsymbol{u}} \frac{1}{2}\|\tilde{\boldsymbol{A}}\boldsymbol{u} - \boldsymbol{y}\|_2^2 + \lambda\|(\boldsymbol{c_1}, \boldsymbol{c_2}, \ldots, \boldsymbol{c_\kappa})\|_{TV_{1-D}} \tag{8}$$

Here, $\tilde{\boldsymbol{A}} = (a_{ij})$ where $j \in \boldsymbol{U}$, and $\boldsymbol{c_k} = (u_{j \in \boldsymbol{C_k}})$ where $\boldsymbol{C_k} \subset \boldsymbol{U}$ denotes the set of pixel indices included in component k. Therefore, $\bigcup_{k=1}^{\kappa} \boldsymbol{C_k} = \boldsymbol{U}$. Let $\boldsymbol{c}$ denote the reordered $\boldsymbol{u}$ by concatenating $\boldsymbol{c_k}$s, so 1-D TV of it is simply defined as:

$$\|\boldsymbol{c}\|_{TV_{1-D}} = \sum_j |\boldsymbol{c_j} - \boldsymbol{c_{j-1}}| \tag{9}$$

In Fig. 2, the line profiles of the same 500-pixel segment taken from the intermediate reconstructed and segmented update pixels (estimated in the first and the second iterations of the algorithm) are compared with the corresponding pixels of the ground truth given in Fig. 1(a), in order to envisioning the idea behind our 1-D TV-based reconstruction. The segment is falling into a single connected component, say $\boldsymbol{C_k}$. First, the update pixels found after one iteration of TV reconstruction ($\boldsymbol{u}^{(1)}_{j \in \boldsymbol{C_k}}$) are plotted together with the original gray levels ($\boldsymbol{x}^{*}_{j \in \boldsymbol{C_k}}$). The second graph shows how excessively fluctuating update pixels in Fig. 2(a) are segmented ($\boldsymbol{s}^{(1)}_{j \in \boldsymbol{C_k}}$). Lastly, the third graph is obtained by performing one-sweep 1-D TV reconstruction ($\boldsymbol{u}^{(2)}_{j \in \boldsymbol{C_k}}$) on the previous sequence of update pixels and segmenting them ($\boldsymbol{s}^{(2)}_{j \in \boldsymbol{C_k}}$). It shows that, even in the second iteration, the signal is closely approximated.

Once the connected components are determined, they are arranged in vector form. While arranging, the way we trace the pixels within a component has influence on the results. Various contour tracing algorithms might be performed here, but they yield

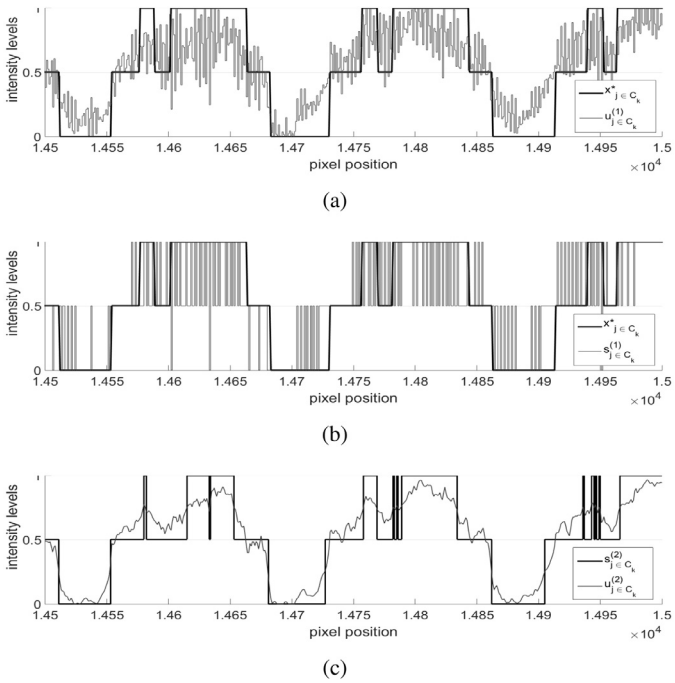

Fig. 2. 500-pixel line profiles taken from (a) the original phantom and vectorized update pixels falling into a connected component in the first iteration, (b) again the original phantom together with the discretized update pixels, and (c) one-sweep TV-regularized update pixels with their discretization results.

extra computational load. In this paper, we simply trace the pixels in column-major and row-major order, interchangeably. For every 100 iterations, periodically, we change the direction from vertical to horizontal, or vice versa. Also both in Eqs. (7) and (8), the regularization parameter λ has a crucial importance. While using low valued λ defeats the purposed of using TV regularization, using high valued λ may oversmooth and yield degenerated object boundaries, even the noise is finely suppressed. In [20], $\lambda \in [2^{-4}, 2^{-13}]$ is the suggested range.

3.2. Estimating segmentation parameters

When the labels are known in advance, using the simple thresholding technique used by DART seems to be producing highly accurate results. However, when the labels are not known and the only prior knowledge is the number of labels, the algorithm should also perform a procedure in order to estimate the labels. In [11], such a procedure, called projection distance minimization (PDM), is proposed. It iteratively minimizes the current projection distance (referring to the Euclidean distance in the sinogram domain), with respect to the gray levels first when the thresholds are given, and the thresholds later while the gray levels are kept fixed. In this subsection, we expand the proposed algorithm by suggesting a new automatic segmentation procedure. We exploit the idea of PDM while devising a formulation to estimate the gray levels (see Section 3.2.1), and proposed a two-stage procedure which makes use of both the gray level histogram and the sinogram, to select thresholds (see Section 3.2.2).

3.2.1. Estimating labels

In this subsection, we devise a formulation by differentiating the projection error to find the minima. The resulting equation will be used to update the labels in each iteration.

Projection error at any iteration is defined as $E = \|\boldsymbol{b} - \tilde{\boldsymbol{b}}\|_2^2$, which gives the squared Euclidean distance between the observed data $\boldsymbol{b}$ and the forward projection $\tilde{\boldsymbol{b}} = \boldsymbol{As}$, where $\boldsymbol{s}$ is the current seg-

mented estimate. Since each pixel intensity is restricted to be an element of the label set $\boldsymbol{s}_j \in \mathcal{L}$, E can be rewritten as follows:

$$E = \sum_{i=1}^{M} (\boldsymbol{b}_i - \sum_{l=1}^{L} \xi_l \boldsymbol{Q}_{il})^2 \quad \text{where} \quad \boldsymbol{Q}_{il} = \sum_{j \in \boldsymbol{\Omega_l}} a_{ij} \tag{10}$$

where $\boldsymbol{\Omega}_l = \{j | \boldsymbol{s}_j = \xi_l\}$, the index set of the pixels whose intensities are set to ξ_l. Since Eq. (10) is differentiable to ξ_ls, each new ξ_k can be updated by using the remaining ξ_ls, such that the projection error is minimized. By rewriting E in terms of ξ_k and the associated $\boldsymbol{Q}_{ik}$, one comes up with the following solution:

$$\frac{\partial E}{\partial \xi_k} = \frac{\partial}{\partial \xi_k} \left\{ \sum_{i=1}^{M} \left(\boldsymbol{b}_i - \left[\sum_{\substack{l=1 \\ l \neq k}}^{L} \xi_l \boldsymbol{Q}_{il} + \xi_k \boldsymbol{Q}_{ik} \right] \right)^2 \right\} = -2 \sum_{i=1}^{M} \left(\boldsymbol{b}_i \boldsymbol{Q}_{ik} - \boldsymbol{Q}_{ik} \sum_{\substack{l=1 \\ l \neq k}}^{L} \xi_l \boldsymbol{Q}_{il} - \xi_k \boldsymbol{Q}_{ik}^2 \right) = -2 \sum_{i=1}^{M} \boldsymbol{Q}_{ik} \left(\boldsymbol{b}_i - \sum_{\substack{l=1 \\ l \neq k}}^{L} \xi_l \boldsymbol{Q}_{il} \right) + 2 \xi_k \sum_{i=1}^{M} \boldsymbol{Q}_{ik}^2 \tag{11}$$

where $k \in \{1, 2, \ldots, N\}$. Therefore, each label ξ_k can easily be estimated by equalizing Eq. (11) to 0 and solving it, as follows:

$$\xi_k = \frac{\sum_{i=1}^{M} \boldsymbol{Q}_{ik} (\boldsymbol{b}_i - \sum_{\substack{l=1 \\ l \neq k}}^{L} \xi_l \boldsymbol{Q}_{il})}{\sum_{i=1}^{M} \boldsymbol{Q}_{ik}^2}. \tag{12}$$

After each iteration, with a discrete reconstruction at hand, the labels are updated by Eq. (12). The non-negativity constraint is applied by directly assigning the negative estimates to 0.

3.2.2. Estimating thresholds

PDM shows that selecting the thresholds which minimizes the projection distance produces more satisfying results [11]. However, the objective function here is not differentiable to the thresholds and a costly simplex search is performed. At that point, limiting the search space to a set of candidate thresholds might be reasonable. In this subsection, we offer to select those candidates by using a histogram-based approach, which is valley estimation. Valley estimation constitutes the first stage of our threshold estimation procedure. The second stage depends on a ranking performed among the candidates. It performs exhaustive search by successively trying each candidate threshold group, and finds the one minimizing $J(\boldsymbol{x})$ in Eq. (6), when the image $\boldsymbol{x}$ is quantized by using it.

In [25], a histogram valley estimation procedure was proposed to determine the number of clusters in order to make a histogram-based segmentation process automatic. In our algorithm, we use these valleys to select the candidate thresholds. The valley estimation algorithm can briefly be reviewed as follows [25]:

(1) The normalized histogram binning is performed for the reconstructed image $\boldsymbol{x}$ by dividing its normalized histogram into 32 bins, each of which is containing 8 gray levels.
(2) Each bin is assigned to a probability according to the following rules:

$$P(\boldsymbol{G_i}) = \begin{cases} 0, & \text{if} (\boldsymbol{H_i} > \boldsymbol{H_{i-1}}) \vee (\boldsymbol{H_i} > \boldsymbol{H_{i+1}}), \\ 1/4, & \text{if} (\boldsymbol{H_i} < \boldsymbol{H_{i-1}}) \wedge (\boldsymbol{H_i} = \boldsymbol{H_{i+1}}), \\ 3/4, & \text{if} (\boldsymbol{H_i} = \boldsymbol{H_{i-1}}) \wedge (\boldsymbol{H_i} < \boldsymbol{H_{i+1}}), \\ 1, & \text{if} (\boldsymbol{H_i} < \boldsymbol{H_{i-1}}) \wedge (\boldsymbol{H_i} < \boldsymbol{H_{i+1}}), \\ P(\boldsymbol{G_{i-1}}), & \text{if} (\boldsymbol{H_i} = \boldsymbol{H_{i-1}}) \wedge (\boldsymbol{H_i} = \boldsymbol{H_{i+1}}). \end{cases} \tag{13}$$

where $\vee$ denotes "logical or", $\wedge$ denotes "logical and" operators, $\boldsymbol{G_i}$ and $\boldsymbol{H_i}$ denote the bins and the corresponding pixel distributions, respectively. Here, $i \in \{2, 3, \ldots, 31\}$ since $P(\boldsymbol{G_1}) = P(\boldsymbol{G_{32}}) = 0$.
(3) Finally, the histogram is scanned in the reversed direction and the bins whose probabilities exceed 1 when summed to the adjacent ones are also updated to be 1. The probabilities of the remaining bins, which could not be set to 1, are directly set to 0.

Once the valleys are found as the bins whose probabilities are 1, our algorithm simply selects the means of those bins as candidate thresholds. Let $\boldsymbol{\tau_{cdt}}$ denote the set of the candidate thresholds, here and hereafter.

In the second stage, the collection of the $(L-1)$-element ordered subsets of the candidate thresholds (defined as $\mathcal{T} = \{\boldsymbol{\tau} : \boldsymbol{\tau} \in \mathcal{P}(\boldsymbol{\tau_{cdt}}) \wedge |\boldsymbol{\tau}| = (L-1)\}$, where $L = |\mathcal{L}|$) is considered as search space. Here, τ denotes a *candidate threshold group*. The number of the elements included by this collection is $|\mathcal{T}| = \binom{|\boldsymbol{\tau_{cdt}}|}{L-1}$, meaning we have that many candidates to try. The optimum threshold group is selected among $\boldsymbol{\tau} \in \mathcal{T}$s as the one which minimizes $J(\boldsymbol{x})$ in Eq. (6). Let $\boldsymbol{\tau_{opt}}$ denote this optimum group of thresholds, and $\boldsymbol{x}_{\boldsymbol{\tau_{opt}}}$ denote the image segmented by using $\boldsymbol{\tau_{opt}}$. The same notation applies for the other thresholds $\boldsymbol{\tau}$.

Furthermore, to prevent high fluctuations, a control operation is carried out before deciding to use $\boldsymbol{\tau_{opt}}$ for segmentation. This operation checks the relative difference between the current cost resulting from $J(\boldsymbol{x})$ by using the selected threshold group, and the cost resulting from the previous threshold (say $\boldsymbol{\tau}^{(\boldsymbol{k-1})}$). If the difference is bigger than a predefined tolerance ϵ, the algorithm keeps using the previous threshold group instead of the optimal one. In fact, we take the risk of switching the thresholds with the new ones at the expense of going away from the minima, unless the relative distance is less than a tolerance. So the current threshold $\boldsymbol{\tau}^{(\boldsymbol{k})}$ becomes either $\boldsymbol{\tau_{opt}}$ or $\boldsymbol{\tau}^{(\boldsymbol{k-1})}$, as defined below:

$$\boldsymbol{\tau}^{(\boldsymbol{k})} = \begin{cases} \boldsymbol{\tau_{opt}}, & d(\boldsymbol{\tau_{opt}}, \boldsymbol{\tau}^{(\boldsymbol{k-1})}) < \epsilon \\ \boldsymbol{\tau}^{(\boldsymbol{k-1})}, & \text{otherwise} \end{cases} \tag{14}$$

where $d(\boldsymbol{\tau_{opt}}, \boldsymbol{\tau}^{(\boldsymbol{k-1})})$ denotes the relative distance defined as:

$$d(\boldsymbol{\tau_{opt}}, \boldsymbol{\tau}^{(\boldsymbol{k-1})}) = \frac{J(\boldsymbol{x}_{\boldsymbol{\tau_{opt}}}) - J(\boldsymbol{x}_{\boldsymbol{\tau}^{(\boldsymbol{k-1})}})}{J(\boldsymbol{x}_{\boldsymbol{\tau_{opt}}})} \tag{15}$$

Here the suggested ϵ is found as 10^{-3}.

In Fig. 3(b), an intermediary continuous reconstruction from 10 projections of the ground truth in Fig. 3(a) is shown. It is obtained by performing the sequence of 2-D TV minimization, Otsu's segmentation, label estimation, 1-D TV regularization on the update pixels, respectively. Then, the image is segmented by using simple thresholding used by DART (c), Otsu's thresholding (d) and the proposed thresholding (d) schemes. Fig. 3(b) is neither resembling

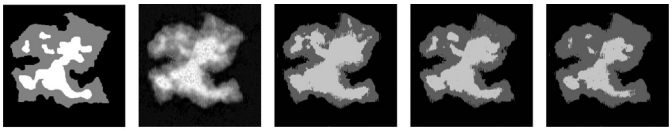

(a) - (b) - (c) .595 (d) .641 (e) .666

Fig. 3. Comparison of simple thresholding, Otsu's thresholding and the proposed thresholding: (a) original phantom, (b) an intermediary reconstruction from 10 projections of (a), (c) simple thresholding by using the average of two consecutive gray levels on (b), (d) Otsu's segmentation on (b), (e) the proposed segmentation on (b).

Proposed Threshold Estimation Procedure

function: τ_{opt} = threshold($x, \mathcal{L}$)
$\tau_{cdt} \leftarrow$ valley_estimation(x)
$\mathcal{T} \leftarrow \{\tau : \tau \in \mathcal{P}(\tau_{cdt}) \wedge |\tau| = |\mathcal{L}| - 1\}$
$\tau_{opt} \leftarrow \underset{\tau \in \mathcal{T}}{\text{argmin}}\ J(x_\tau)$
end

Fig. 4. The pseudo code of the proposed optimum threshold selection procedure.

Proposed D-TVIRT Algorithm

$x^{(0)} \leftarrow$ TVreconstruction($x := 0, A, b$)
$k := 0, \quad p \in [0, 1]$
while (termination criterion is not met) **do**
  if ($\mathcal{L}$ is not known)
    $\tau^{(k)} \leftarrow$ threshold_estimation($x^{(k)}, |\mathcal{L}|$)
    $s^{(k)} \leftarrow$ segmentation($x^{(k)}, \mathcal{L}^{(k)}, \tau^{(k)}$)
    $\mathcal{L}^{(k+1)} \leftarrow$ label_estimation($s^{(k)}, \mathcal{L}^{(k)}$)
  else
    $s^{(k)} \leftarrow$ segmentation($x^{(k)}, \mathcal{L}$)
  end
  $U \leftarrow \varnothing, f^{(k)} \leftarrow s^{(k)}, u^{(k)} \leftarrow 0$
  for $j \leftarrow 1 : n$
    if ($\exists h \in N(j) : s_h^{(k)} \neq s_j^{(k)}$) $\vee$ ($rand() < p$)
      $U \leftarrow U \cup \{j\}$
      $f_j^{(k)} \leftarrow 0$
      $u_j^{(k)} \leftarrow x_j^{(k)}$
    end
  end
  $\ell^{(k)} \leftarrow$ connected_component_labelling(U)
  $c^{(k)} \leftarrow u_{\ell^{(k)}}^{(k)}$ s.t. $c^{(k)} = (c_1^{(k)}, c_2^{(k)}, \ldots, c_\kappa^{(k)})$
    where $c_i^{(k)} = u_{(\ell^{(k)}=i)}^{(k)}$
  $r^{(k)} \leftarrow b - Af^{(k)}$
  $u^{(k)} \leftarrow$ 1D_TVreconstruction($c^{(k)}, A_I, r^{(k)}$)
  $x^{k+1} \leftarrow (f^{(k)} + u^{(k)}) * G_\sigma$
end

Fig. 5. The pseudo code of the proposed D-TVIRT algorithm.

to the ground truth (due to the incorrect intermediary gray levels) nor to the continuous reconstruction. Since Otsu's thresholding is more elaborate than selecting the values in the middle, in terms of segmentation, Fig. 3(c) better represents the continuous input image, however it is also not that good at representing the ground truth, since it does not use any prior knowledge on it. Fig. 3(e), on the other hand, better represents the ground truth, even though the labels are not approximated to the correct values yet. Their similarities to the ground truth are measured by using the structural similarity (SSIM) index, and the results are placed under the images. Lastly in Fig. 4, the pseudo code of the proposed threshold estimation procedure is given.

3.3. Overall algorithm: D-TVIRT

In Fig. 5, the pseudo-code and in Fig. 6, the flowchart of the overall algorithm are given. Fig. 6 starts from the observed sinogram which will be the input for the TV-regularized reconstruction. We denote this inversion phase as "TV reconstruction". Once the inversion is performed, the obtained real-valued image is segmented. If the labels are known a priori, only the thresholds are determined as the middle values of the consecutive two gray levels. We denoted this procedure as "simple threshold selection" in the flowchart. Otherwise, if the labels are not known, the labels and the thresholds are separately estimated. Initial thresholds are determined by using Otsu's thresholding and the initial labels are set as the mean of each cluster formed after thresholding. For the succeeding iterations, thresholds are selected among the candidates corresponding to the valleys on the reconstructed image's gray-level histogram. Then, a collection consisting of the ordered subsets of the candidates is constructed and the optimum subset is selected as the one which minimizes the objective functional. We denote this procedure as "threshold estimation" in both flowchart and the pseudo code. Once the image is segmented according to the thresholds, the gray levels are updated to be used in the next iteration. This part is referred to as "label estimation". Until a stop condition is satisfied, a new initial set of pixels (update pixels), therefore a new projection matrix (with only the weights contributed by the update pixels), and a new vector of projection measures (residual sinogram) are all prepared for the subsequent reconstruction phase. In the pseudo code segment where the set of update pixels is constructed, $N(j)$ denotes the 8-neighbors of the pixel j. After those steps are performed, the update pixels are stacked into a vector and 1-D TV (referred to as "1D TV reconstruction") is performed on it. Before jumping back to the segmentation step, updated pixels are merged with the fixed pixels and the result is smoothed by a Gaussian filter G_{sigma}.

4. Simulation experiments

In this section, the experimental results obtained by the proposed D-TVIRT algorithm are presented and compared with the SART, the TVmin (which stands for continuous TV minimization algorithm), and the DART algorithms. The results produced by the conventional FBP also take place in the graphical interpretations, just to provide insight on the weakness of analytical methods when the observed data is highly limited. All implementations are done in Matlab. The DART algorithm is implemented as described in [10]. AIR Tools Matlab package [26] is exploited for the simulation of the parallel beam projection and the SART algorithm. FBP is performed using inverse Radon transform (*iradon*) function with linear interpolation and Ram-Lak filter with a cut-off of 100% Nyquist frequency. The reconstructed images of the FBP, the SART and the TVmin algorithms are segmented using Otsu's thresholding [27], in order to have a label-based solution. Furthermore, to solve the TV minimization problem either for D-TVIRT or for TVmin, the publicly available TVAL3 solver [20] is used.

The structural similarity index (SSIM), proposed in [28], and misclassification percentage (MP), given in Eq. (16), are two main metrics used for the performance evaluation.

$$\text{MP}(\%) = \frac{100}{N}\sum_{j=1}^{N} 1 - \delta(\boldsymbol{x}_j, \boldsymbol{x}_j^*) \tag{16}$$

where $\delta(\boldsymbol{x}_j, \boldsymbol{x}_j^*) = \begin{cases} 1, & \boldsymbol{x}_j = \boldsymbol{x}_j^* \\ 0, & \boldsymbol{x}_j \neq \boldsymbol{x}_j^* \end{cases}$ and $\boldsymbol{x}^*$ denotes the reconstructed image.

In addition to them, relative number of misclassified pixels (rNMP) is preferred in segmentation parameter estimation experiments (in Section 4.4), since the results produced by our algorithm are directly compared to the results obtained by the PDM-DART in [11], where rNMP is used for quantification. rNMP is defined as the fraction of the misclassified pixels with respect to the total number of pixels. Since we use rNMP when the labels are not known and

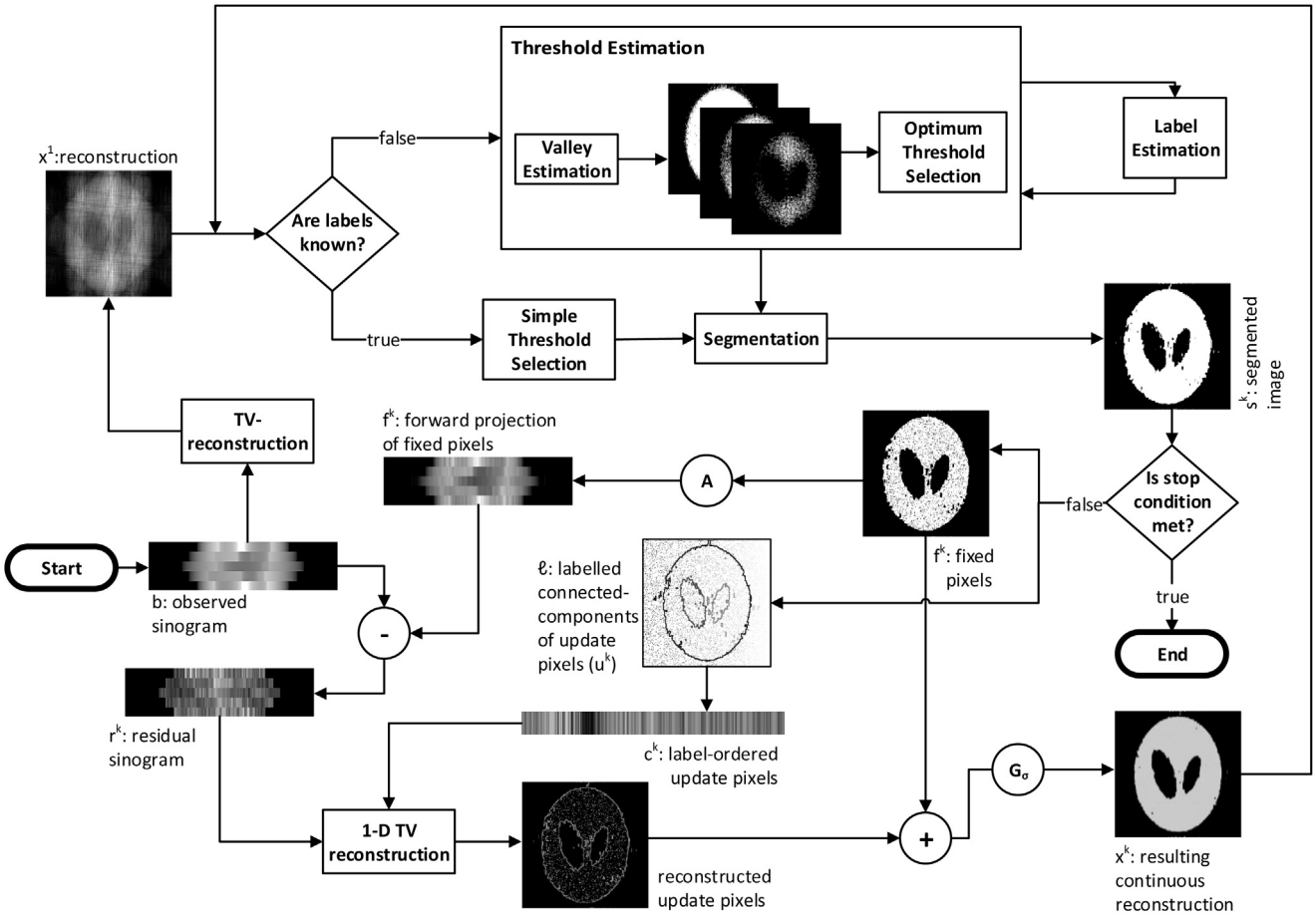

Fig. 6. A schematic overview of the proposed D-TVIRT algorithm (this flowchart is inspired from the flowchart of PDM-DART [11]).

Fig. 7. Ground truth phantom images used in the experiments: (a) Phantom-1, (b) Phantom-2, (b) Phantom-3, (b) Phantom-4 and (e) Phantom-5.

since the estimated labels may differ from the originals, the estimated labels of the pixels are mapped to the closest ground truth labels before measuring rNMP.

The synthetic phantom images used in the experiments are given in Fig. 7. First two phantoms are binary with $\mathcal{L} = \{0, 1\}$, while the other three are multi-labeled, where both Phantom-3 and Phantom-5 with $\mathcal{L} = \{0, 0.5, 1\}$, and Phantom-4 with $\mathcal{L} = \{0, 0.25, 0.5, 0.75\}$. Phantom-1, 2 and 3 are adapted from [11][10], respectively, Phantom-4 is produced, and Phantom-5 is taken from the phantom gallery of AIR Tools. The sizes of Phantom-1 and 2 are 512×512, while the others are all 256×256. The *fix probability* parameter of both the DART and the D-TVIRT algorithms is set to $p = 0.85$, unless otherwise stated. In all experiments, the random seed used in the DART algorithm is kept and the same seed, therefore the same sequence of random numbers, is used in the D-TVIRT for randomly selected update pixels. The radius for the Gaussian smoothing filter is selected as $\sigma = 3$ pixels. The algorithms are run until convergence. Convergence is defined as having a relative difference, between the costs from two consecutive iterations, less than or equal to $10e-6$. The maximum number of iterations for both the SART and the TVmin algorithms is set to 500. On the other hand, the minimum and maximum number of iterations for DART and D-TVIRT are set as $K_{min} = 200$ and $K_{max} = 2000$. For D-TVIRT algorithm, 10 iterations of initial SART, and for each main iteration, 5 sub-iterations of SART are performed. Similarly, the number of initial TVmin iterations and the number of subsequent 1-D TVmin iterations are set as 5 and 5, respectively. The regularization parameter $\lambda = 2^{-13}$ is used in TVmin. In D-TVIRT, while $\lambda_0 = 2^{-13}$ is used for the initial 2-D TV based reconstruction, $\lambda_k = 2^{-10}$ is tuned for the subsequent 1-D TV reconstructions, unless otherwise stated.

Four different scenarios are considered through the following four subsections. In the first three, we assume that the gray levels are already known, therefore the proposed segmentation parameter estimation modules will be inactive. Later, in Section 4.4, we present the utility of those modules by considering the scenario of not having a priori knowledge on the labels.

4.1. Limited number of projections

A "projection" refers to the detector values collected from single angle. In all experiments presented here, we use $\sqrt{(N)}$ (512 for Phantom-1 and 2; 256 for the others) detector values per angle. The projections are sampled equidistantly. In this experiment, we assume that the projection measurements are noiseless.

In Fig. 8, the SSIM scores obtained from five methods are plotted as a function of the number of projections, gradually increasing from 2 to 6 for Phantom-1, and 2 to 12 for the other Phantom-2, 3 and 4. In Fig. 9, the images that are reconstructed from various number of projections by using all the algorithms except FBP are

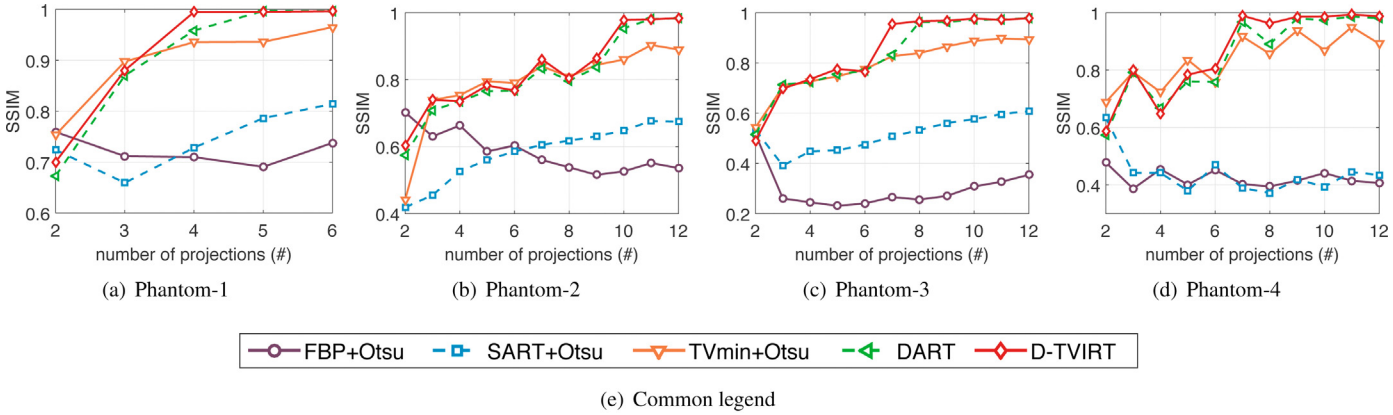

Fig. 8. Comparison of FBP, SART, TVmin, DART and D-TVIRT algorithms in terms of SSIM scores, with respect to various number of projections.

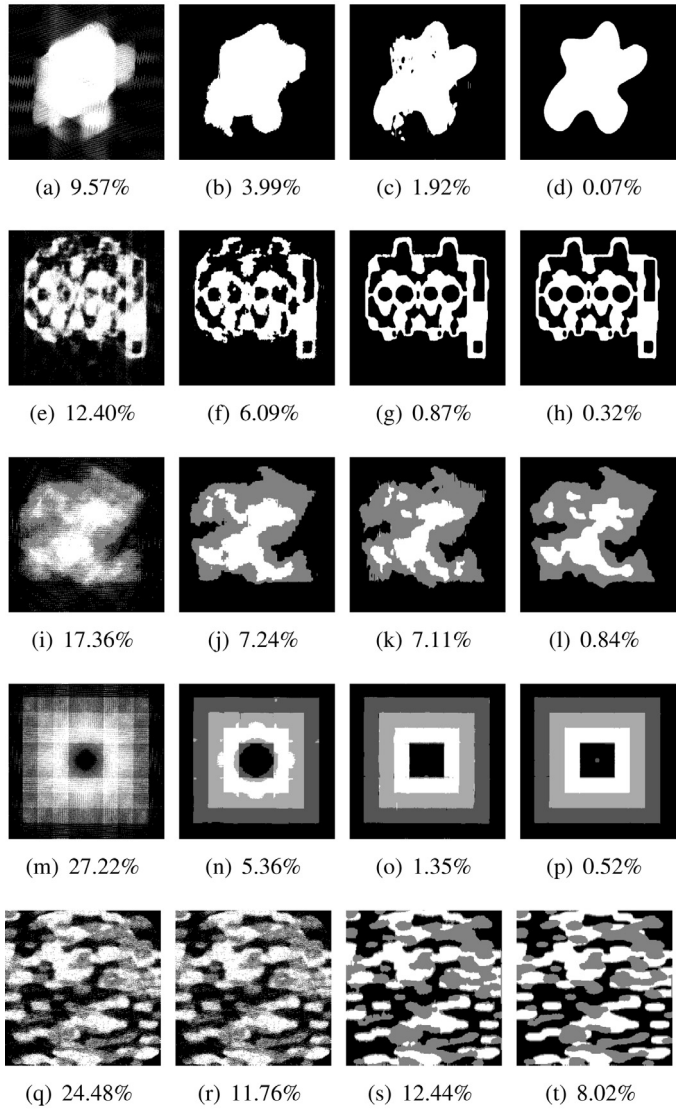

Fig. 9. A visual comparison of reconstruction results of SART (first column), TVmin (second column), DART (third column) and D-TVIRT (last column) algorithms for a certain number of projections: $d = 4$ for Phantom-1 (first row), $d = 10$ for Phantom-2 (second row), $d = 7$ for Phantom-3 (third row), $d = 7$ for Phantom-4 (forth row) and $d = 30$ for Phantom-5 (last row), with their corresponding MP(%)'s below.

shown. For each phantom, the number of projections are selected as the minimum that yields an almost perfect reconstruction according to the visual judgement, by at least one of the algorithms. The MP(%) score of each reconstruction is shown under the image.

4.2. Limited view problem

In this set of experiments, limited view problem in tomography is simulated. Limited view refers to limited angular range, positioned centrally in the full angular range (180°, say from 0° to 180°). In this section, we assume the projections are measured at 1° intervals through the angular range, which we denote with θ. For instance, if $\theta = 40$, then it means that the beams are acquired from each 1° interval within the range from 70° to 110°.

In Fig. 10, the SSIM scores obtained from five methods are plotted as a function of various angular ranges. In Fig. 11, again the reconstruction examples for various angular ranges are shown, with their MP(%) scores stated below.

4.3. Noisy projections

In the former subsections, noise-free projection measurements were used. In this section, the robustness of each algorithm with respect to the noise are experimented. In order to simulate a noisy projection, the projection samples are polluted by adding white Gaussian noise with various SNR values in dB (from 0 to 40) on them. The *fix probability* is set to 0.5 in this section, since it yields more accurate reconstructions for both the DART and the D-TVIRT, when the noise is the case. The results given in Fig. 12 are obtained by using various number of noisy projections acquired either from full, or from limited angular range. In Fig. 13, the reconstructed images obtained by using different settings combining the noisy projection scenario either with the limited number of projections or with the limited view, are shown.

4.4. Lack of prior knowledge on gray levels

In this subsection, we test the D-TVIRT algorithm together with the proposed threshold estimation and the label update steps, on Phantom-1, which is also used to evaluate PDM-DART in [11]. As stated before, the initial thresholds are determined by Otsu's thresholding, and the labels are initialized by the mean value of each cluster. In this section, λ_k is set to 2^{-8}, while λ_0 is still 2^{-13}.

In Fig. 14, D-TVIRT reconstructions of Phantom-1 from 3, 4 and 5 projections are given. Their reconstruction performances, in terms of rNMP, are shown in Table 1. The gray levels of the resulting reconstructions are also stated in the same table.

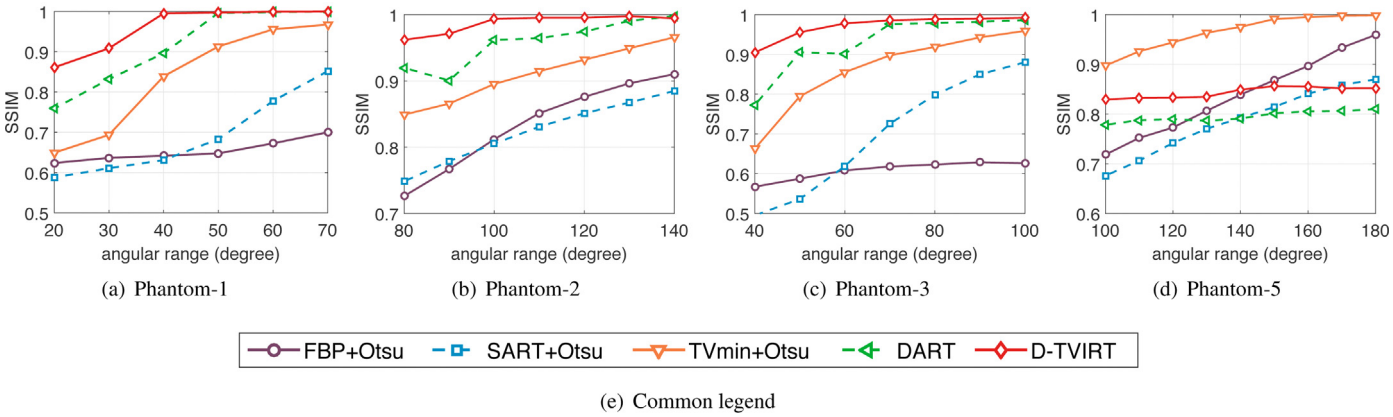

Fig. 10. Comparison of FBP, SART, TVmin, DART and D-TVIRT algorithms in terms of SSIM score with respect to the various angular ranges.

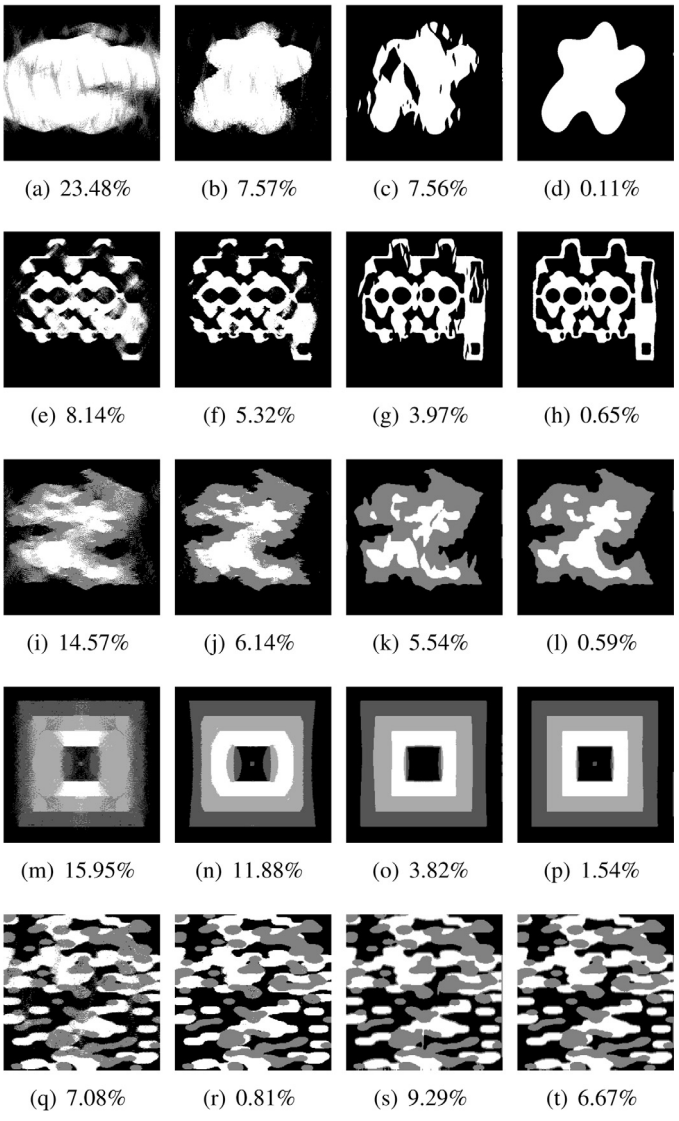

Fig. 11. A visual comparison of reconstruction results of SART (first column), TVmin (second column), DART (third column) and D-TVIRT (last column) algorithms for a certain angular range: $\theta = 40$ for Phantom-1 (first row), $\theta = 100$ for Phantom-2 (second row), $\theta = 60$ for Phantom-3 (third row), $\theta = 120$ for Phantom-4 (forth row), $\theta = 140$ for Phantom-5 (last row), with their corresponding MP(%)'s below.

Table 1
Comparison of performances of PDM-DART and D-TVIRT on Phantom-1, when the labels are not known a priori, in terms of rNMP. The labels estimated by D-TVIRT are also placed in the last column.

d	PDM-DART	D-TVIRT	Estimated Labels
3	0.2117	0.0608	{0, 0.9892}
4	0.1057	0.0025	{0, 0.9911}
5	0.0008	0.0016	{0.0021, 1}
6	0.0008	0.0012	{0.0003, 0.9998}
7	0.0004	0.0006	{0, 0.9999}

4.5. Computational cost

Finally, in Table 2, the run times of the DART and the proposed algorithm are compared. The entities are the averaged run times of each experiment presented in Figs. 8, 10 and 12 . The experiments are performed on a 3.40 GHz Core 8 computer with 4 GB of memory.

As the results show, D-TVIRT is unfortunately requiring more computational time than DART. The gap increases for the experiments whereas the D-TVIRT shows reasonably better performance, such as limited view experiments. For such experiments, one can infer that the DART converges earlier than the D-TVIRT by getting stuck in the local minima, while TV regularization enforces D-TVIRT to keep searching. In the noisy projection experiments, the differences between the average run times of the algorithms are getting larger, such that receiving an estimate from D-TVIRT takes roughly 3 times more than DART, except the experiments performed on Phantom-3 whereas D-TVIRT is 6 times slower than DART. Here, another observation is that, as the number of boundary, and therefore update pixels increases (as in Phantom-3), the convergence of D-TVIRT gets slower, since the size of TV minimization problem also increases.

For the segmentation parameters estimation experiment, the computational cost increases, since the threshold selection procedure also contributes with $O\left(\begin{matrix}|\tau_{cdt}|\\ \mathcal{L}-1\end{matrix}\right)$ time complexity to the algorithm. To give an insight, the reconstruction of Phantom-1 from $d = 4$ projections took 916.06 s, while it was 688.02 s when the labels are known. The same experiment lasts 58.82 s when performed by DART which converges in 248 iterations without approximating well.

5. Discussion

In the previous section, we analyzed the proposed algorithm and compared it with the segmented FBP, SART, TVmin algorithms, and the DART algorithm. We performed four separate set of experiments by considering four different scenarios, and based on those

Table 2
Comparison of run times of (I) DART and (II) D-TVIRT in seconds computed by averaging each run of the experiments presented in Figs. 8, 10 and 12 .

Phantom	Limited number of projections		Limited view		Noisy projections	
	(I)	(II)	(I)	(II)	(I)	(II)
1	246.25	550.73	376.30	895.60	66.71	234.07
2	225.01	356.46	334.90	998.26	174.86	555.41
3	83.32	86.90	171.97	368.45	50.82	273.48
4	50.05	91.33	100.44	335.13	111.43	332.47
5	66.82	288.10	99.00	774.48	136.77	838.67

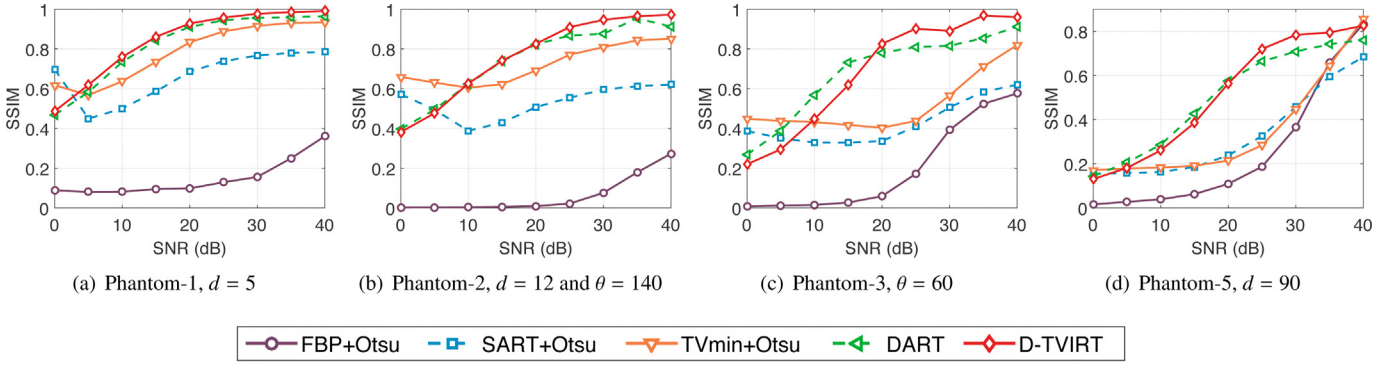

(a) Phantom-1, $d = 5$ (b) Phantom-2, $d = 12$ and $\theta = 140$ (c) Phantom-3, $\theta = 60$ (d) Phantom-5, $d = 90$

(e) Common legend

Fig. 12. Comparison of FBP, SART, DART and D-TVIRT algorithms in terms of SSIM score with respect to various SNRs in dB.

experiments, the following discussions are drawn. Except for the fact that the computational load of the FBP method is very low when compared to the iterative methods, as it is obvious from the majority of the results, it is not comparable with the other algorithms, when the data is limited. As it can be seen from the noisy projection experiments, FBP is also highly sensitive to the noise. Although the reconstruction quality of the SART algorithm seems better than FBP in most of the experiments interpreted by graphs, SART is also not capable enough to recover an image from its incomplete projections. The TVmin, on the other side, exhibited prominently better reconstructions than FBP and SART, even in some cases, it produced quite comparable or even better results than DART and D-TVIRT, as in limited view experiment performed on Phantom-5 (see Fig. 10(d) and the last row of Fig. 11). However, due to the imperfect projections, the results obtained by SART and TVmin algorithms tend to have artefacts during the inversion, which frequently mislead the post processing segmentation step.

When we compare DART and D-TVIRT, it is observed that, in almost all experiments, D-TVIRT reached a SSIM score around 1, with fewer or at worst roughly same amount of data; except the experiments performed on Phantom-5, which couldn't be reconstructed in a satisfactory way by both algorithms, even full angular range was used (Fig. 10(d)). Even though the SSIM curves in the limited number of projections experiments are close to each other; the visual comparisons may provide insight on the improvement revealed by D-TVIRT. By visual judgement, DART was not that successful in reconstructing Phantom-1 from $d = 4$, and Phantom-3 and 4 from $d = 7$ projections. Actually, the utility of D-TVIRT is more significant in limited view experiments. D-TVIRT was able to produce almost perfect reconstructions from the angular ranges $\theta = 40$, $\theta = 100$ and $\theta = 60$ for Phantom-1, 2 and 3, respectively. D-TVIRT reveals a reasonable improvement on DART, when the projections are acquired through a limited angular range. In the noisy projections experiments, the D-TVIRT yielded either same with or slightly better results than the DART for the settings used in Fig. 12, but when the SNR values are above 20 dB. According to the several experiments, some of which we didn't place here, DART is more robust to the noise when the angular range is full but the number of projections are limited. This proposition arises from the observation that the DART performs at the same level with D-TVIRT, although it wasn't the case when the same number of noise-free projections are used. But again D-TVIRT outperforms DART in the noisy projection experiments where the angular range is narrowed down.

When the gray levels are not known in advance, D-TVIRT optimizes the segmentation parameters by alternating between label estimation and threshold estimation stages. Its ability of estimating those parameters are evaluated by reconstructing Phantom-1 from various number of projections, and comparing the results with PDM-DART by referring to [11]. D-TVIRT nearly managed to reach rNMP goal 0.001 by only using $d = 4$ projections, while it was reached by $d = 5$ by PDM-DART in [11]. When the run times discussed in Section 4.5 are also taken into account, since the computational load that is brought forth by the proposed algorithm is high but acceptable, one can adequately prefer to use D-TVIRT instead of DART, due to its ability to produce better reconstructions under more limited conditions. However the computational load arises as the main drawback of D-TVIRT, that should be improved in the future studies. Apart from this drawback, the way we are arranging the update pixels in an order to treat as a 1-D signal can also be improved. Various contour tracing algorithms (e.g. Moore-neighbor tracing) may yield better results, while revealing additional cost.

6. Conclusion

In this paper, we focussed on the problem of tomographic reconstruction from incomplete projections, and with respect to this, we proposed an algorithm which incorporates the DART algorithm (that is in use in the field of discrete tomography) and well-known TV minimization technique. Our approach embeds TV-based regularization into the stages of the DART, in order to improve its capabilities. The DART algorithm employs decoupled sequences of inversion using an algebraic reconstruction method, and discretization using a simple global thresholding scheme. Our algorithm first comes up with the idea of regularization using TV measure

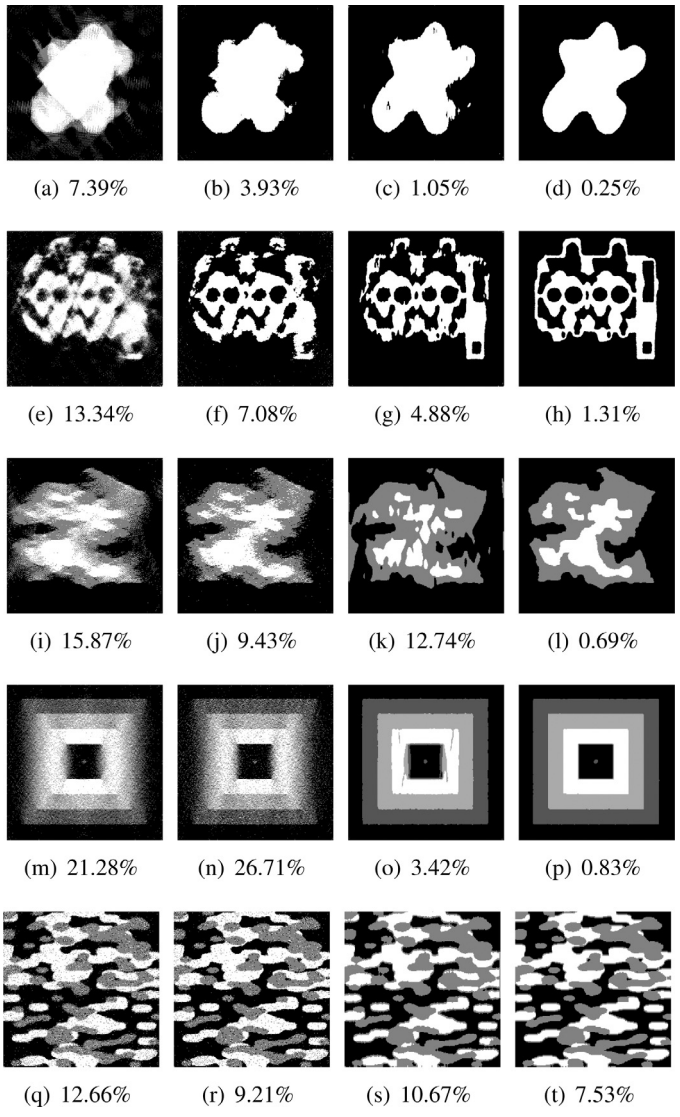

Fig. 13. A visual comparison of reconstruction results of SART (first column), TVmin (second column), DART (third column) and D-TVIRT (last column) algorithms for certain SNR values: 35 *dB* for Phantom-1 using $d = 5$ (first row), 32 *dB* for Phantom-2 using $d = 12$ and $\theta = 140$ (second row), 35 *dB* for Phantom-3 using $\theta = 60$ (third row), 32 *dB* for Phantom-4 using $\theta = 140$ (forth row) and 35 *dB* for Phantom-5 using $d = 90$ (last row), with their corresponding MP(%)s below.

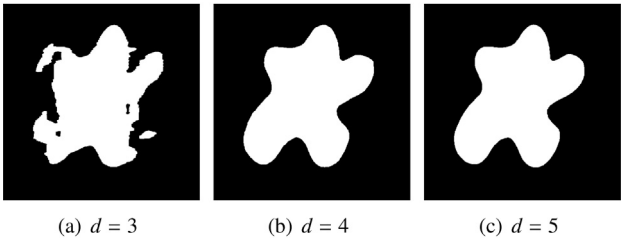

Fig. 14. D-TVIRT reconstructions with segmentation parameter estimation modules, for various number of projections.

throughout the inversion stages of the DART, while keeping the discretization as it is. For that purpose, both 2-D and 1-D TV-based regularizations are exploited. While 2-D TV is used to estimate the initial guess, which is a complete image; 1-D TV is used to reconstruct a disjointed subset of the image pixels, which contains the only pixels to be updated within the subsequent iterations. As a second contribution, we proposed a two-stage threshold selection procedure to be used if the gray levels are not known in advance. We suggested to use both histogram based thresholding and exhaustive minimization of TV regularized projection error. We evaluated our algorithm by realizing the scenarios of limited number of projections, limited view, noisy projections and lack of a priori knowledge on gray levels, for different phantoms and different settings. The results show that the proposed D-TVIRT algorithm improves the DART algorithm in terms of the reconstruction quality at the expense of additional computational time.

References

[1] A.C. Kak, M. Slaney, Principles of Computerized Tomographic Imaging, IEEE Press, 1988.
[2] A.H. Andersen, A.C. Kak, Simultaneous algebraic reconstruction technique (SART): a superior implementation of the art algorithm, Ultrason. Imaging 6 (1) (1984) 81–94.
[3] C.L. Byrne, Iterative Optimization in Inverse Problems, CRC Press, 2014.
[4] A. Kuba, G. Hermann, Discrete Tomography: Foundations, Algorithms, and Applications, vol. 61, 1999, pp. 199–221.
[5] G.T. Herman, A. Kuba, Advances in Discrete Tomography and Its Applications, Springer Science & Business Media, 2008.
[6] D. Gale, et al., A theorem on flows in networks, Pacific J. Math. 7 (2) (1957) 1073–1082.
[7] K.J. Batenburg, A network flow algorithm for reconstructing binary images from continuous X-rays, J. Math. Imaging Vision 30 (3) (2008) 231–248.
[8] A. Tuysuzoglu, W.C. Karl, I. Stojanovic, D. Castanon, M.S. Unlu, Graph-cut based discrete-valued image reconstruction, IEEE Trans. Image Process. 24 (5) (2015) 1614–1627.
[9] H.Y. Liao, G.T. Herman, A coordinate ascent approach to tomographic reconstruction of label images from a few projections, Discr. Appl. Math. 151 (1) (2005) 184–197.
[10] K.J. Batenburg, J. Sijbers, Dart: a practical reconstruction algorithm for discrete tomography, IEEE Trans. Image Process. 20 (9) (2011) 2542–2553.
[11] W. van Aarle, K.J. Batenburg, J. Sijbers, Automatic parameter estimation for the discrete algebraic reconstruction technique (DART), IEEE Trans. Image Process. 21 (11) (2012) 4608–4621.
[12] L.I. Rudin, S. Osher, E. Fatemi, Nonlinear total variation based noise removal algorithms, Physica D: Nonlinear Phenom. 60 (1) (1992) 259–268.
[13] A. Chambolle, An algorithm for total variation minimization and applications, J. Math. Imaging Vision 20 (1–2) (2004) 89–97.
[14] A. Beck, M. Teboulle, Fast gradient-based algorithms for constrained total variation image denoising and deblurring problems, IEEE Trans. Image Process. 18 (11) (2009) 2419–2434.
[15] A. Beck, M. Teboulle, A fast iterative shrinkage-thresholding algorithm for linear inverse problems, SIAM J. Imaging Sci. 2 (1) (2009) 183–202.
[16] T. Goldstein, S. Osher, The split Bregman method for l1-regularized problems, SIAM J. Imaging Sci. 2 (2) (2009) 323–343.
[17] C. Wu, X.-C. Tai, Augmented Lagrangian method, dual methods, and split Bregman iteration for ROF, vectorial TV, and high order models, SIAM J. Imaging Sci. 3 (3) (2010) 300–339.
[18] B. Wahlberg, S. Boyd, M. Annergren, Y. Wang, An admm algorithm for a class of total variation regularized estimation problems, IFAC Proc. Vol. 45 (16) (2012) 83–88.
[19] S. Ramani, J.A. Fessler, A splitting-based iterative algorithm for accelerated statistical X-ray CT reconstruction, IEEE Trans. Med. Imaging 31 (3) (2012) 677–688.
[20] C. Li, W. Yin, Y. Zhang, User's guide for TVAL3: TV minimization by augmented Lagrangian and alternating direction algorithms, CAAM Rep. 20 (2009) 46–47.
[21] X. Zhuge, W.J. Palenstijn, K.J. Batenburg, TVR-DART: a more robust algorithm for discrete tomography from limited projection data with automated gray value estimation, IEEE Trans. Image Process. 25 (1) (2016) 455–468.
[22] D.L. Donoho, Compressed sensing, IEEE Trans. Inform. Theory 52 (4) (2006) 1289–1306.
[23] E.J. Candès, J. Romberg, T. Tao, Robust uncertainty principles: exact signal reconstruction from highly incomplete frequency information, IEEE Trans. Inform. Theory 52 (2) (2006) 489–509.
[24] E. Demircan-Tureyen, M.E. Kamasak, A compressed sensing based approach on discrete algebraic reconstruction technique, in: Engineering in Medicine and Biology Society (EMBC), 2015 37th Annual International Conference of the IEEE, IEEE, 2015, pp. 7494–7497.
[25] D.-Y. Huang, T.-W. Lin, W.-C. Hu, Automatic multilevel thresholding based on two-stage Otsu's method with cluster determination by valley estimation, Int. J. Innov. Comput. Inform. Control 7 (10) (2011) 5631–5644.
[26] P.C. Hansen, M. Saxild-Hansen, Air tools – a Matlab package of algebraic iterative reconstruction methods, J. Comput. Appl. Math. 236 (8) (2012) 2167–2178.
[27] N. Otsu, A threshold selection method from gray-level histograms, Automatica 11 (285–296) (1975) 23–27.
[28] Z. Wang, A.C. Bovik, H.R. Sheikh, E.P. Simoncelli, Image quality assessment: from error visibility to structural similarity, IEEE Trans. Image Process. 13 (4) (2004) 600–612.